

The geochemical and petrological characteristics of prenatal caldera volcano: a case of the newly formed small dacitic caldera, Hijiori, Northeast Japan

Isoji Miyagi¹  · Noriko Kita² · Yuichi Morishita³

Received: 5 October 2016 / Accepted: 17 July 2017 / Published online: 18 August 2017
© The Author(s) 2017. This article is an open access publication

Abstract Evaluating the magma depth and its physical properties is critical to conduct a better geophysical assessment of magma chambers of caldera volcanoes that may potentially cause future volcanic hazards. To understand pre-eruptive conditions of a magma chamber before its first appearance at the surface, this paper describes the case of Hijiori caldera volcano in northeastern Japan, which emerged approximately 12,000 years ago at a place where no volcano ever existed. We estimated the depth, density, bulk modulus, vesicularity, crystal content, and bulk H₂O content of the magma chamber using petrographic interpretations, bulk and microchemical compositions, and thermodynamic calculations. The chemical mass balance calculations and thermodynamic modeling of the erupted magmas indicate that the upper portion of the Hijiori magmatic plumbing system was located at depths between 2 and 4 km, and had the following characteristics: (1) pre-eruptive temperature: about 780 °C; (2) bulk magma composition: 66 ± 1.5 wt% SiO₂; (3) bulk magmatic H₂O: approximately 2.5 wt%, and variable characteristics that depend on depth; (4) crystal content: ≤57 vol%; (5) bulk modulus of magma: 0.1–0.8 GPa; (6) magma density: 1.8–2.3 g/cm³; and (7) amount of excess magmatic H₂O: 11–32 vol% or 48–81 mol%. The range of

melt water contents found in quartz-hosted melt inclusions (2–9 wt%) suggests the range of depth phenocrysts growth to be wide (2~13 km). Our data suggest the presence of a vertically elongated magma chamber whose top is nearly solidified but highly vesiculated; this chamber has probably grown and re-mobilized by repeated injections of a small amount of hot dacitic magma originated from the depth.

Keywords Prenatal volcano · Hijiori · Melt inclusions · Magmatic H₂O · Rhyolite-MELTS

Introduction

According to the Japan Meteorological Agency, 110 volcanoes are currently listed as active volcanoes in the country. An active volcano is defined as having erupted in the last 10,000 years or that currently exhibits active fumarolic vents (JMA 2013). These volcanoes have potential to erupt again in the future. To mitigate potential impacts on our lives related to the future volcanic events, histories of active volcanoes along with volcanic hazard maps are compiled (e.g., NIED 2013) or online databases established (e.g., the United States Geological Survey Volcano Hazards Program).

However, in a long-term planning of land development covering long timescales (e.g., tens to hundreds of thousands of years), it is inevitable to consider the possibility of future appearances of volcanoes that may cause lethal impacts on infrastructures and human lives in areas, where active volcanoes have not been previously known to exist.

To understand initial behavior of volcanoes in a region that is volcanically inactive, we focused on some newly formed explosive volcanoes in the northeastern part of Japan. These include Ichinome-gata volcano at 39°57'33"N 139°44'25E (Kano et al. 2011; Katsui et al. 1979), Hijiori volcano

Communicated by Gordon Moore.

✉ Isoji Miyagi
miyagi.iso14000@aist.go.jp

¹ Geological Survey of Japan, Tsukuba Central 7, 1-1-1 Higashi, Tsukuba, Ibaraki 305-8567, Japan

² Department of Geoscience, University of Wisconsin-Madison, Weeks Hall, 1215 W Dayton St, Madison, WI 53706, USA

³ Department of Geosciences, Shizuoka University, 836, Ohya, Shizuoka 422-8529, Japan

at 38°36'35"N 140°9'20"E (Kawaguchi and Murakami 1994; Miyagi 2007; Sugimura 1953; Ui 1971), Adachi volcano at 38°13'15"N 140°39'02"E (Kanisawa and Yoshida 1989), and Zenikame volcano at 41°44'21"N 140°51'05"E (Hasegawa and Suzuki 1964; Yamagata et al. 1989). Among the volcanoes, Hijiori is one of the most well studied with regard to its petrography, eruption age determination, description of eruptive sequence, bulk eruptive volume, topography, and caldera structure. Therefore, Hijiori volcano was selected as an appropriate example of a newly formed explosive volcano to understand the depth and physical properties of the magma plumbing system prior to its first appearance to the surface.

Detection of potential volcanoes and prediction of their future activities will be based largely on geophysical exploration techniques (e.g., Umeda et al. 2006). However, knowledge of petrological, geochemical, and physical properties of magma storage conditions (depth, temperature, density, bulk modulus, size, shape, etc.) can improve the interpretation of geophysical data and as a result increase the reliability in the prediction of future volcanism. In doing so, we will estimate the pressure, temperature and bulk magmatic H₂O content using the geochemical compositions of bulk rocks, phenocrysts and melt inclusions in combination with the MELTS program (Asimow and Ghiorso 1998; Ghiorso and Sack 1995; Gualda et al. 2012).

Hijiori volcano

Hijiori, one of the active volcanoes in Japan, first erupted about 12,000 years ago at a site where no volcanic activity had been previously known to exist (Kawaguchi and Murakami 1994; Miyagi 2007, 2004; Sugimura 1953; Ui 1971; Ui et al. 1973). The volcano is located at 38°36'35"N 140°9'20"E, about 40 km west of the Tohoku (Northeast) volcanic front within the Japan Arc (Fig. 1), near the boundary of the No. 4 hot finger. These so-called hot fingers are the locally developed hot regions within the mantle wedge of subduction zone that have a shape of 50-km-wide inclined finger. Above these, Quaternary volcanoes in Northeast Japan form 10 clusters (Tamura et al. 2002).

Hijiori, a small caldera with a diameter of approximately 2 km, has subsided about 200 m. At present, the caldera floor is located about 350 m above the sea level. The volcano was systematically studied when a geothermal energy project funded by the New Energy and Industrial Technology Development Organization began drilling in and around the caldera (NEDO 1983). The drill core records indicated that the caldera had undergone piston-cylinder-type subsidence (Miyagi 2007; NEDO 1983).

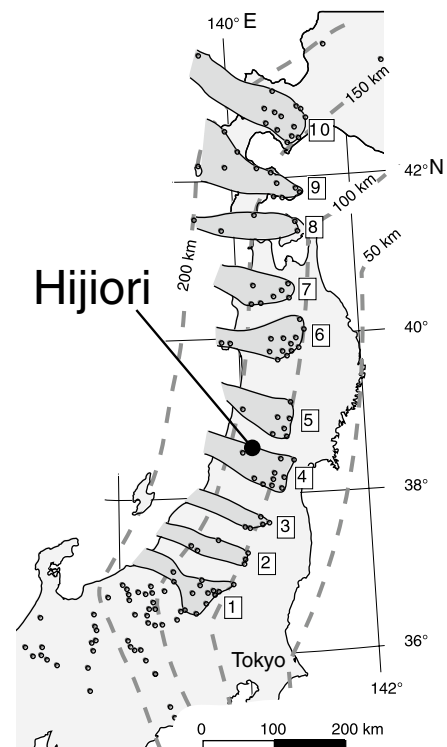


Fig. 1 Hijiori volcano is located at the northeastern Japan arc, close to the boundary of the so-called No. 4 hot finger (one of the gray-filled regions proposed by (Tamura et al. 2002)

Hijiori volcano erupted in four major stages, produced valley-filling pyroclastic flow deposits and air-fall tephra with bulk volumes of 1.4 and 0.6 km³, respectively (Kawaguchi and Murakami 1994; Miyagi 2007). The eruptive activities seem to have ended shortly after the initial eruption as there is no significant difference in the ¹⁴C ages between eruption stage 1 and stage 3, evidently the length of each hiatus was not long enough to produce black soils in between (Miyagi 2004). The volume of the caldera subsidence is estimated to be approximately 0.8 km³, which is nearly equivalent to the estimated volume of erupted magma [0.83 km³ dense-rock equivalent (DRE), excluding the bulk volume of caldera-fill deposits and the volume of the Komat-subuchi lava dome (Miyagi 2007)].

Samples and analytical methods

Petrography

The Hijiori volcanic samples include white, porphyritic pumices and lithic fragments. The pumice fragments

being essential (magmatic) material (Miyagi 2007) were targeted for sampling and analysis. These fragments sometimes contain matrix glass and phenocrysts of plagioclase, quartz, hornblende, orthopyroxene, magnetite, and ilmenite. The matrix is colorless, transparent, and crystal poor. There is no significant difference in the texture of the matrix in pumices formed during the four Hijiori eruptive stages, except for some variation in the porosity; relative to stage 1 pumice, stage 2 pumice is less vesicular (about <30 vol%), but those in stage 3 and 4 show a relatively high vesicularity (about >70 vol%) pumice (Miyagi 2007).

The phenocryst assemblage is generally constant throughout the four stages of volcanic activity. Plagioclase is the most abundant phenocryst in the Hijiori eruptive products. The phenocrysts are present in both pumice and as single crystals in the matrix of pyroclastic flow deposits. The size of the phenocrysts is up to 1 by 0.2 mm, although this size may be underestimated as larger plagioclase phenocrysts observed so far are always broken. The smaller plagioclase phenocrysts are more euhedral than the larger phenocrysts. Plagioclase, hornblende, and magnetite sometimes occur as aggregates (see below). Lithic accessory fragments are also present. They have the same mineral assemblage as the Hijiori magma but the minerals are finer than phenocrysts in Hijiori pumice and possess granular textures and no interstitial melt. These fragments are termed as clots in this study.

Amphibole is the second most abundant phenocryst in the Hijiori eruptive products. The crystals are mostly euhedral, with sizes up to 1 by 0.5 mm, present in both pumice and as individual crystals in the matrix of pyroclastic flow deposits. Quartz, the third most abundant phenocryst up to 2 mm in diameter, is generally euhedral, sometimes partly corroded or occurred as broken fragments. The phenocrysts are mostly present as individual crystals in pyroclastic flow deposit.

A small amount of orthopyroxene phenocrysts is also found in the Hijiori eruptive products. These phenocrysts are euhedral with the largest size being approximately 1 mm.

Small-sized oxide minerals such as magnetite and ilmenite are also present as aggregates (Fig. 2g) or as individual crystals.

These phenocrysts occasionally include silicate melt inclusions (MIs). MIs range from a few to hundreds of micrometers in diameter. However, larger MIs are only found in quartz phenocrysts where they are located not only near dissolution boundaries but also deep inside the dark core of the phenocrysts (Fig. 2d). Binocular microscopic investigations show that MIs in quartz crystals collected from air-fall pumices are colorless, transparent, and crystal-free.

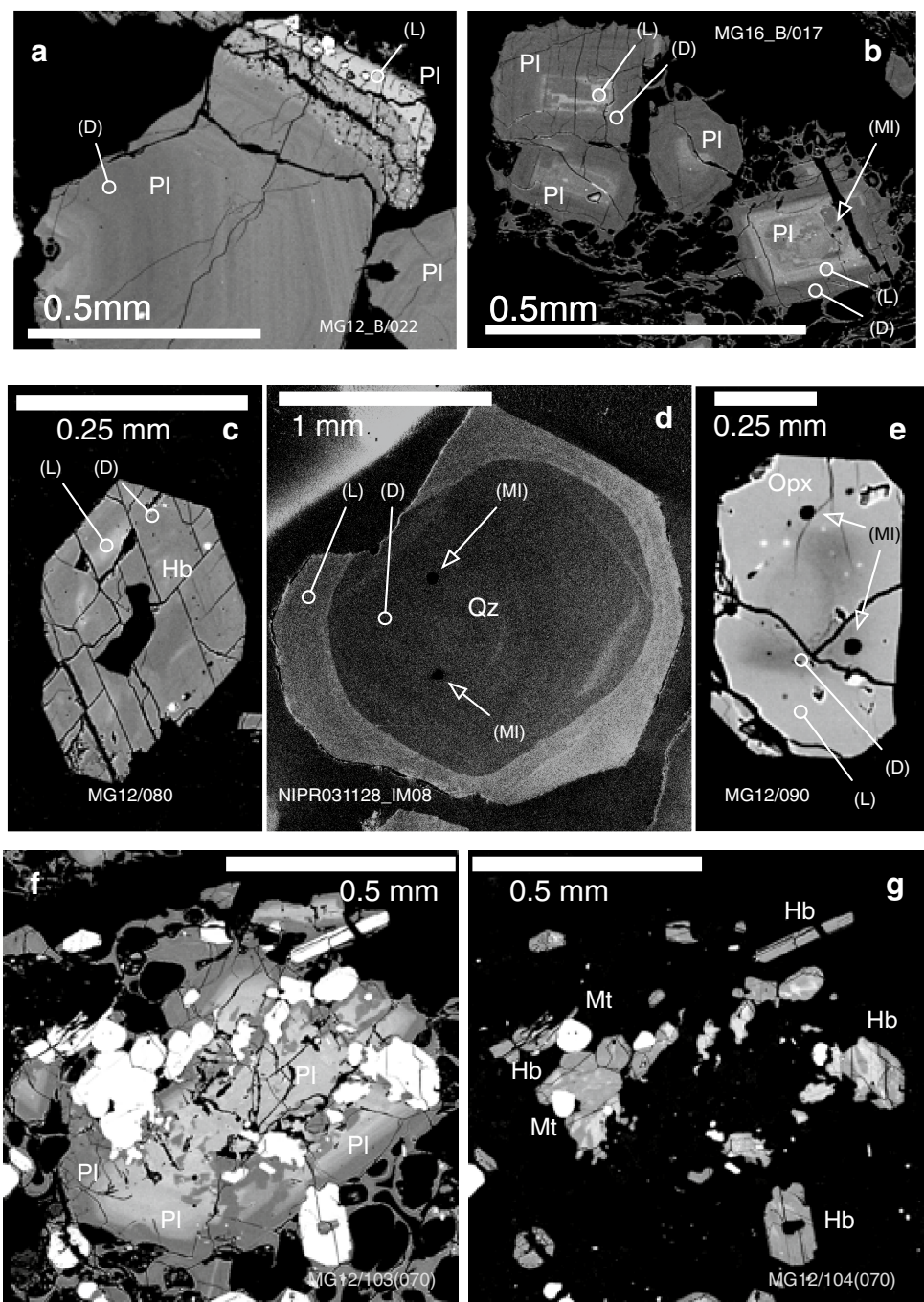
In contrast, those collected from relatively thick pyroclastic flow deposits are opaque, suggesting that these MIs have undergone post-eruptive devitrification associated with slow cooling (e.g., Skirius et al. 1990), thus being excluded from this study. MIs were also found in plagioclase and amphibole phenocrysts. The MIs are concentrated in patchy cores or reverse-zoned bands, but almost absent from oscillatory zoned or zoning-free areas.

Analytical procedures

Samples were washed ultrasonically in purified water for 30–120 min and were dried overnight in an oven at 90 °C. They were sieved at 32.0, 16.0, 4.0, 1.0 and 0.7 mm sizes before phenocrysts were hand-picked for analysis. Only phenocrysts surrounded by clear glass were chosen for micro-analysis. Bulk rock major element compositions were determined on mixed sample Li-metaborate/tetraborate glass beads by X-ray fluorescence (XRF) by Activation Laboratories Ltd. (Ancaster, Canada). The sampling method and sample preparation for analysis in this study are both described by Miyagi et al. (2012).

The electron probe microanalyzer (EPMA) and secondary ion mass spectrometry (SIMS) analysis was performed on uncrushed samples to avoid fracturing of phenocrysts. The phenocrysts were mounted on a glass disk (thickness = 5 mm, diameter = 24 mm) in a single, close-packed layer using an as small as possible amount of resin to minimize degassing in the vacuum chamber during analysis. This approach is an improvement relative to metallic mounting agents, such as indium (e.g., Hauri et al. 2002), that cause interference during backscattered electron microscope imaging as a result of the high backscatter coefficient of the metal relative to typical rock-forming minerals. Backscattered electron images (BEIs) of the samples obtained using a JEOL JXA-8900 scanning electron microscope (SEM) at the Geological Survey of Japan (GSJ) with an electron acceleration of 15 kV, a probe current of 12 nA, and a probe diameter of 1 μm were carefully examined before analysis. An image of the entire polished surface was constructed as a mosaic of digital BEIs with a size of 1000 \times 1000 pixels (pixel size of 1 \times 1 μm). Each BEI was captured using at least two different brightness and contrast settings, one to optimize viewing plagioclase and MIs, and the other for hornblende and pyroxene (e.g., electric supplementary material: ESM_1_Hj_MG42_BEIs). In addition to the BEIs, cathodoluminescence images (CLs) of quartz phenocrysts were obtained using a JEOL JSM-5900LV SEM, with an electron acceleration of 15 kV, a probe current of 2 nA, and a Gatan MINI-CL detector at the National Institute of Polar Research, Tachikawa, Tokyo, Japan.

Fig. 2 Scanning electron images of phenocrysts. **d** is cathode-ray luminescence image, and the rest of figures are backscattered electron image. *Pl* plagioclase, *Qz* quartz, *Hb* hornblende, *Opx* orthopyroxene, *Mt* magnetite. **a** Relatively large broken fragments of a plagioclase phenocryst with a calcium-rich rim. **b** Relatively small euhedral plagioclase phenocrysts with a calcium-rich core inside. **c** An euhedral hornblende phenocryst cut perpendicular to the *c*-axis, with light (*L*) and dark (*D*) parts. **d** An euhedral quartz phenocryst, with a dark (*D*) corroded core and light (*L*) mantle. **e** An euhedral orthopyroxene phenocryst with blurred normal zoning. **f** An aggregate of plagioclase, hornblende, and magnetite. **g** The same view as **f** with a different brightness condition suitable for hornblende



Major element compositions (Si, Ti, Al, Fe, Mn, Mg, Ca, Na, K, S, Cl, and F) of phenocrysts and phenocryst-hosted melt MIs were determined using a JEOL JXA-8900 EPMA at the GSJ, Tsukuba, Ibaraki, Japan. These analyses used an accelerating voltage of 15 kV, a probe current of 12 nA, a probe diameter of 4 μm , a wavelength dispersive X-ray spectroscope (WDS), and a ZAF correction. No special techniques were applied to obtain X-ray signals except for Na, S, Cl, and F analysis, given as follows: Na loss associated

with migration during electron bombardment was prevented using the defocused electron probe as well as by analyzing Na in first sequence with a short (4 second) counting time. Counting time was 20-s for Si, Ti, Fe, Ca, and K. The use of a defocused electron probe is one of the efficient ways to minimize Na loss and enhance the Na count (Hamada and Fujii 2007). For the S, Cl, and F analysis, a 50-s counting time was applied to reduce statistical error, yielding a reproducibility that was better than ± 0.02 wt%.

H₂O contents in MIs were determined using a CAMECA IMS-1270 SIMS at the GSJ. This analysis used a 1 nA, homogeneous, Cs⁺ primary beam spot that was restricted to a diameter of 20 μm using a circular aperture. Secondary ions were collected using a total impact energy of 20 kV (primary accelerating voltage of +10 kV; secondary extraction voltage of −10 kV) from the central region via a 10 by 10 μm square mechanical field aperture. An electron gun was used during analysis for charge compensation on the sample surface. Background hydrogen ions were suppressed using energy filtering by positioning of the mechanical energy slit (offset by +20 V, with a width of 20 V). H₂O concentrations (in wt%) in MIs were obtained by empirically calibrating ¹H/³⁰Si secondary ion count ratios and independently determining SiO₂ concentrations (also in wt%). The accuracy of this method was estimated to be ±0.5 wt% H₂O, with a within-run precision better than ±0.2 wt% H₂O (Miyagi and Yurimoto 1995). The H₂O contents of hornblende along with a number of andesitic and rhyolitic hydrous glass standards were determined by hydrogen gas manometry at the Research Institute of Mining Resources, Akita University, Japan. The accuracy of this method is better than ±0.1 wt%. In addition to SIMS measurements, the H₂O concentrations of MIs were also estimated by subtracting the measured sum of EPMA data from 100 wt% (Devine et al. 1995) using equation (1) of Appendix A in the study by Borisova et al. (2005). The use of EPMA data is to fill in the limitation of the SIMS analysis of MIs having diameters smaller than a few tens of μm.

We conducted a series of thermodynamic calculations for a representative bulk rock composition (“Hj j-Q” in Table 1) using Rhyolite-MELTS (Gualda et al. 2012; Asimow and Ghiorso 1998; Ghiorso and Sack 1995) [1.2.0 (mixed fluid version optimal for mafic and alkalic melts—new H₂O model)]. The ranges of pressures, temperatures, oxygen fugacities, H₂O concentration, and CO₂ concentrations are 0.1 MPa–0.1 GPa at 10 MPa steps, from 700°C to 1400°C at 1°C steps, FMQ to FMQ + 3 log units, 0.1, 0.2, 0.3, 0.4, 0.5, 0.6; 0.7, 0.8, 0.9, 1.0, 1.5, 2.0, 2.5, 3.0, 3.5, 4.0, 4.5, 5.0, 6.0, 8.0, 10 wt% H₂O, and 0.001, 0.010, 0.001 wt% CO₂, respectively. The total number of combinations of these different parameters is approximately 17.6 million per sample. Our own Perl scripts were used to make setting files of the MELTS program, and to automatically run and kill the program 25,200 times per sample. As a results of calculations, several gigabytes of a bunch of csv files were produced, which were further summarized in a series of pressure–temperature plane contour maps and related each other as a set of hyper text documents (electric supplementary material: ESM_4) using our other Perl scripts, a series of GMT programs (<https://www.soest.hawaii.edu/gmt/>, Wessel and Smith 1998), and a series of ImageMagick programs

(<https://www.imagemagick.org>). A part of previous calculation is published in Miyagi (2011).

Results

Phenocryst and glass textures and occurrences

Relatively large plagioclase phenocrysts sometimes show oscillatory zoning (D in Fig. 2a) and also have patchy reaction bands or rims (L in Fig. 2a), similar to those formed during partial dissolution experiments (Nakamura and Shimakita 1998). The majority of smaller and some larger phenocrysts have calcium-rich cores that are sometimes patchy (L in Fig. 2b). Broken plagioclase phenocryst faces are sometimes covered by vesicular matrix glass, suggesting that multiple magma fragmentation events took place before the final event that produced the fragments of pumice in the analyzed samples.

Plagioclase, amphibole, and magnetite sometimes coexist as aggregates (Fig. 2f is optimized for plagioclase and Fig. 2g for hornblende).

Although no zoning was identified in amphibole during optical microscopic examination (Murakami and Kawaguchi 1994), a notable difference in lightness was found during BEI study. The smaller and lighter portions of amphibole (e.g., L in Fig. 2c) are pargasitic (with lower Si and higher Al), whereas the darker majority of amphibole (e.g., D in Fig. 2c) are a variety of magnesio hornblende (with higher Si and lower Al). The lighter, pargasitic portion appears in skeletal or undetermined form, and is enclosed by the darker portion that forms an euhedral outline of the phenocryst. So far, no single pargasitic phenocryst has been identified among the Hijiori eruptive products.

Distinct zoning was observed in quartz phenocrysts from the Hijiori eruptive stage 1 through 4 during the SEM cathodoluminescence imaging study (Fig. 2d). The dark corroded core of a phenocryst (D in Fig. 2) has a sharp boundary with the surrounding lighter rim (L in Fig. 2d) that creates an euhedral outline of the phenocryst. The dark core of the phenocryst appeared reddish during an optical microscopic study using a luminescope, whereas the lighter rim turned bluish.

The analyzed orthopyroxene phenocrysts have normal zoning with dark magnesian cores (D in Fig. 2e) surrounded by a light Fe-rich mantle (L in Fig. 2e).

Chemical composition

The pumice samples are dacite having a narrow range of SiO₂ concentrations (66 ± 1.5 wt%: WR in Fig. 3), and plot in the calc-alkaline field of the SiO₂ vs. FeO/MgO

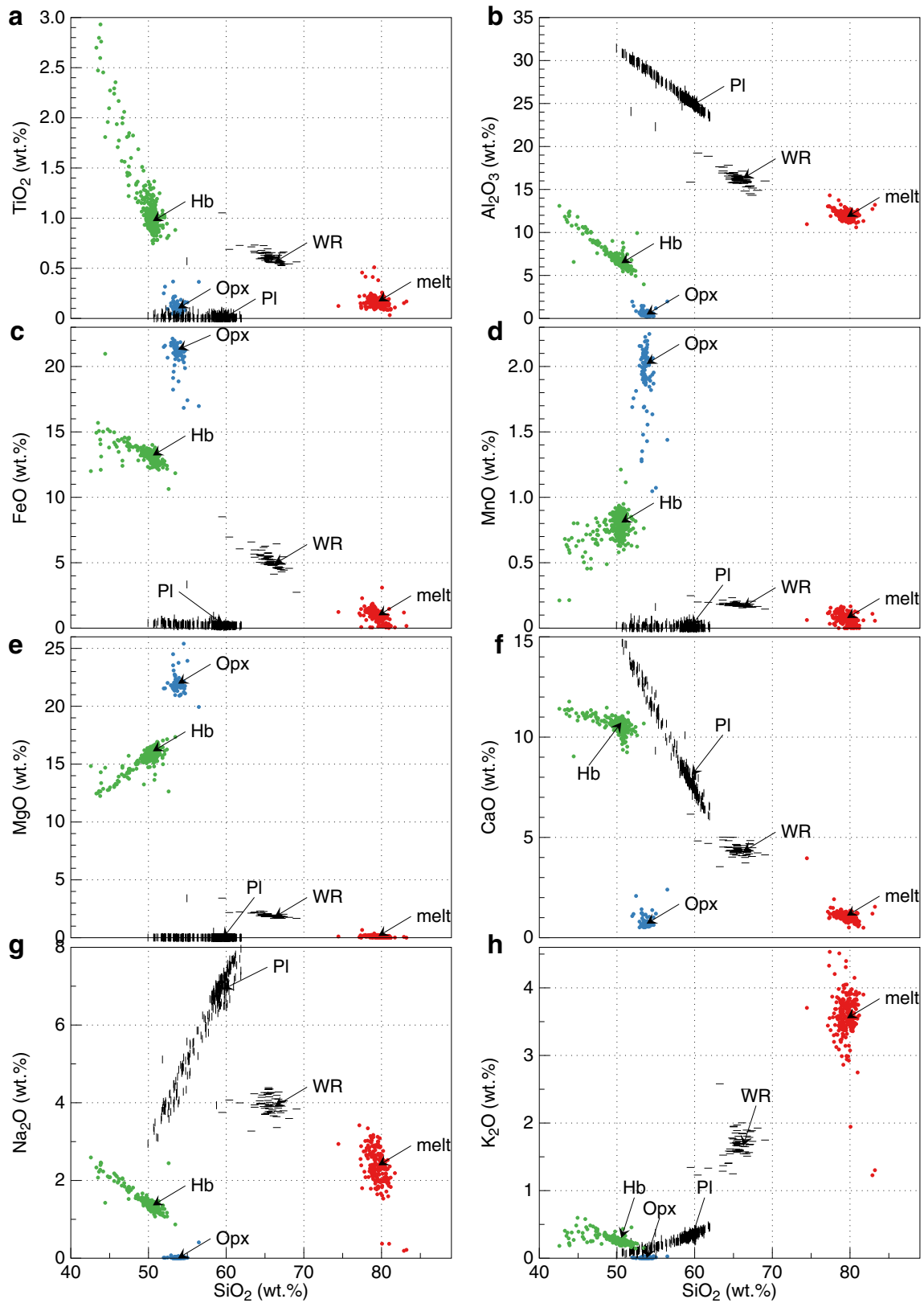


Fig. 3 SiO₂ variation diagrams. WR (horizontal bars): bulk rock pumice (in Table 1), melt (red filled circles): melt inclusions in phenocrysts, Pl (horizontal bars): plagioclase, Hb (green filled circles):

hornblende, Opx (blue filled circles): orthopyroxene, and arrows representative composition of each phase in Table 1

Table 1 Representative chemical composition and the calculated mode.

	hb	opx	pl	qz	mt	il	melt	wr	Hj j-Q	wr(calc)
SiO ₂	51	54	60	100	0	0	80	66	66	66
TiO ₂	1	0.1	0	0	6	50	0.2	0.6	0.6	0.6
Al ₂ O ₃	6.4	0.5	25	0	1.6	0	12	16	16	15
FeO	13	21	0.3	0	83	44	1	5.1	4.9	5.1
MnO	0.8	2.0	0.02	0	0.8	2.1	0.08	0.2	0.2	0.2
MgO	16	22	0	0	0	0	0.15	1.9	1.8	1.9
CaO	11	0.7	8.1	0	0	0	1.1	4.4	4.3	4.8
Na ₂ O	1.4	0	6.9	0	0	0	2.4	4.0	3.9	3.8
K ₂ O	0.3	0	0.3	0	0	0	3.6	1.7	1.7	1.7

Chemical compositions of melt (melt), whole rock (wr), and minerals (*hb* hornblende, *opx* orthopyroxene, *pl* plagioclase, *qz* quartz, *mt* magnetite, *il* ilmenite) are the peak of histograms of their chemistry and are also indicated by arrows in Fig. 3

A pumice sample “Hj j-Q” was selected as a representative of Hijiori magma and was used for the MELTS computations in this study. Weight fraction of melt and minerals (Frac.) are obtained by the method of least squares to find a calculated whole rock composition (wr(calc)) closer to the observed one (wr) by changing the fraction of the melt and minerals. All the figures are described in wt%

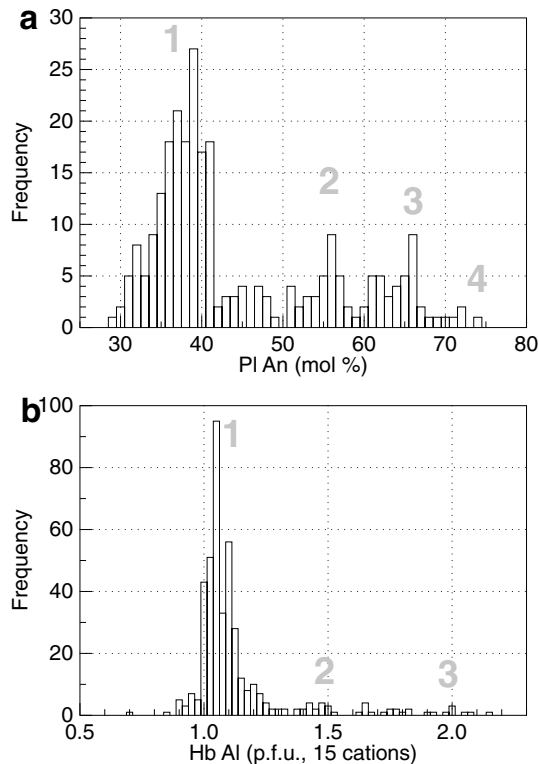


Fig. 4 Chemical composition of plagioclase and hornblende phenocryst from Hijiori volcano. **a** Anorthite composition (An mol %) of plagioclase. **b** Aluminum composition (15 atoms per formula unit) of hornblende. *Gray numbers* are the identifiers of each peak in this paper. Window size (section width) is set to be 1 mol% for An (4a) and 0.025 pfu for Al in hornblende (4b)

diagram of Miyashiro (1974). The chemical compositions of the Hijiori eruptive products did not change throughout the volcanic activity (Ui 1971, and this study), except for the K₂O concentrations that vary slightly between 1.5 and 1.9 wt% in bulk rock samples, and between 3.3 and 4.0 wt% in MIs (Fig. 3h). Except for Na₂O and K₂O the rest of the major oxides show broadly negative correlation with the bulk silica oxides (Fig. 3). Aside from several outliers, the chemical compositions of the whole rock, crystal and melt samples are summarized and shown in Fig. 3 and Table. 1.

Connection between textures and compositions

The plagioclases vary from 30 to 74 anorthite (An) mol% with peaks at 35–41 (Fig. 4a-1), 55 (Fig. 4a-2), and 65–71 An mol% (Fig. 4a-3, a-4). The highest values shown in Fig. 4a-1 is those of large plagioclase phenocrysts having oscillatory zoning (D in Fig. 2a). The other peaks shown in Fig. 4a-2, a-3, and a-4 correspond to the patchy reaction bands or rims of large plagioclase (L in Fig. 2a) and the patchy core of small ones (L in Fig. 2b). The orthopyroxenes show a compositional range between 62 and 70 enstatite (En) mol%, with the majority having compositions of 63–64.5 En mol%. The higher peak corresponds to the light part (L in Fig. 2e) and the lower peak corresponds to the dark Mg-rich core (D in Fig. 2e). The hornblendes are Al poor that peak around 1.1 Al atoms per formula unit (pfu, 15 cations; Fig. 4b-1); although compositions range from 0.7 to

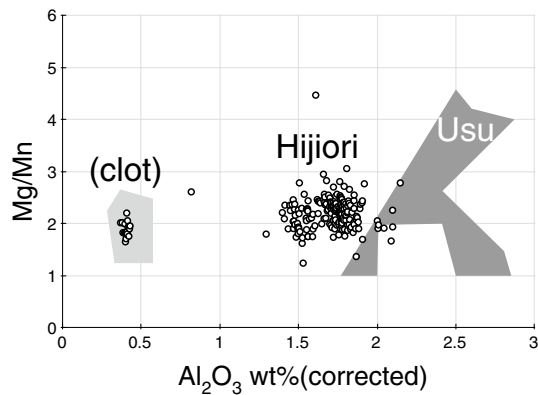


Fig. 5 Chemical composition of magnetite phenocryst from Hijiori volcano. Mg/Mn vs. Al_2O_3 (stoichiometry corrected) composition of magnetite (wt%). Dark gray area “Usu” is those from Usu volcano as a comparison. Light gray area “clot” is those included in lithic fragments with fine granular texture from Hijiori volcano

2.0 (Al, pfu; Fig. 4b-2, b-3). The highest peak in Fig. 4b-1 corresponds to the dark part (D in Fig. 2c), while the rest of the peaks in Fig. 4b-2 and b-3 are the lighter portions having skeletal or undetermined shapes (L in Fig. 2c).

The majority of magnetites have Al_2O_3 varying between 1.4 and 1.9 wt% (stoichiometry corrected; Fig. 5), lower than those in rhyolitic–dacitic eruptive products from Usu volcano (Tomiya and Takahashi 2005). Usu magnetites were reported to associate with eruptive magmatic temperatures estimated to be 780–950 °C. The magnetites with very low Al_2O_3 concentrations (Fig. 5 clot) are found as mineral inclusions in clots (melt-free lithic fragments with fine granular textures).

Phenocryst-hosted MIs from the Hijiori volcano are rhyolitic having SiO_2 concentrations of 79.5 ± 1.5 wt% (Fig. 3, melt), which is one of the highest SiO_2 values in the literature, and they would correspond to very shallow crystallization pressures (Gualda and Ghiorso 2013). Compositions like these are often affected by silicification or secondary hydration (Begue et al. 2014).

There are small but systematic variations in the compositions of the MIs. The relationship may represent that the range of melt compositions of the magma may have changed in time and space during the entrapment. The silica concentrations of the MIs in plagioclase and quartz show two major peaks at $\text{SiO}_2 = 79.0$ and 80.2 wt%, while those in hornblende, orthopyroxene and plagioclase have two smaller peaks at $\text{SiO}_2 = 77.8$ and 79.5 wt%. In addition, the potassium contents in MIs in hornblende, quartz and orthopyroxene are generally lower as compared to those in plagioclase and quartz (see Fig. 6a-2 and -3). At least four peaks of MI H_2O concentrations were identified (Fig. 6b) at 1–3, 4–5, 5–7, and 7–9 wt% where those in quartz-hosted MIs are the

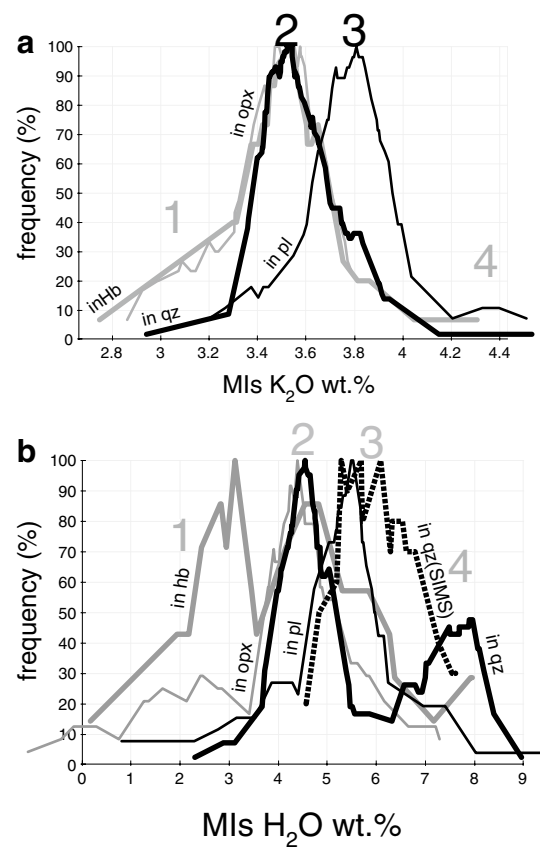


Fig. 6 Frequency of the major element chemistry of melt inclusions (MIs) in phenocrysts. Window size (section width) the frequency diagram is set to be 0.25 and 1 wt% for K_2O (6a) and H_2O (6b), respectively. Gray numbers the identifiers of each peaks. pl (thin black line): in plagioclase host, hb (thick gray line): in hornblende host, opx (thick black line): in orthopyroxene host, qz (thick black line): in quartz host, qz (SIMS) (thick dashed black line): in quartz host, measured by SIMS

highest (6b-4). The carbon concentration in MIs from Hijiori was undetermined.

Discussion

Magma mixing

The textures of plagioclase and quartz phenocrysts in some Hijiori samples indicate that dissolution and recrystallization processes occurred during the magmatism (Fig. 2). Although the bulk rock composition is generally uniform (Fig. 3), the plagioclase, orthopyroxene, and hornblende compositional variations indicate that the magmatism in Hijiori involved at least two end-members having distinct temperatures and/or chemical compositions (Fig. 4). We propose three non-exclusive scenarios that might have happened during the

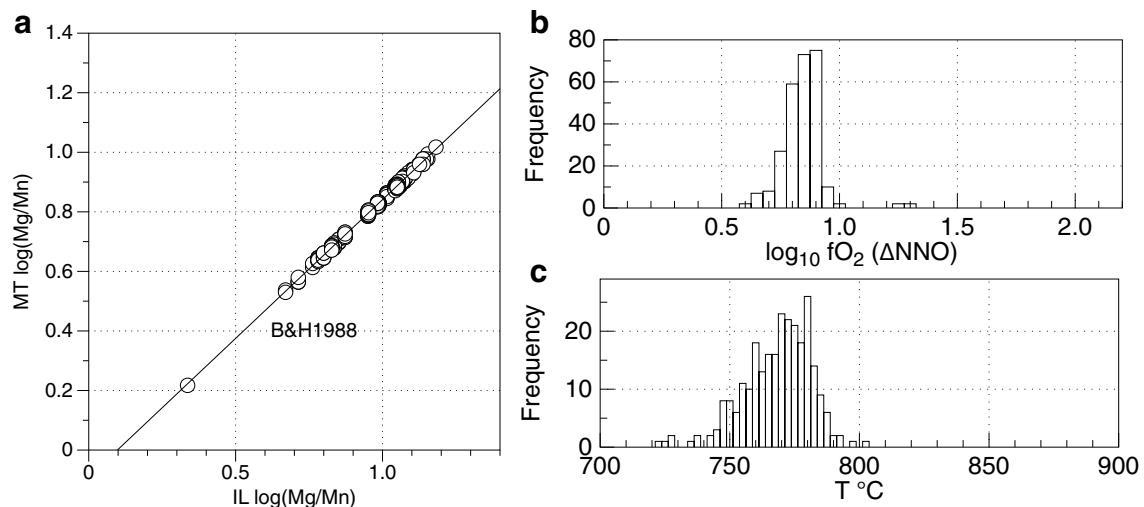


Fig. 7 Fe–Ti minerals. **a** Selected magnetite–ilmenite pairs using Mg/Mn partitioning known as the Bacon and Hirschmann (1988) test. **b** Estimated oxygen fugacity of Hijiori magma by FeTiOxideGeo-

therm (Ghiorso and Evans 2008) using the magnetite–ilmenite pairs that passed the test (a). **c** Histogram of the estimated temperature

magmatism at Hijiori: (1) the magmatism involved geochemically similar end-member magmas but different temperatures, (2) the amount of contaminant was too small to cause significant compositional change (also including the process of thermal transfer without chemical mixing), and/or (3) the mixing ratios of the end-members were constant. Below we will test the scenarios (1) and (2) by focusing on the temperature, pressure, crystal content, and amount of bulk and excess (vapor or supercritical aqueous fluid) magmatic H₂O conditions of the magmatism, using chemical compositions of the bulk rock, phenocryst and MIs to run with the MELTS program. However, it may be difficult to evaluate scenario (3) unless a quantitative end-member magma mixing calculation is solved.

Temperature

The magmatic temperature of the Hijiori magmas during eruption was estimated by FeTiOxideGeotherm 1.1.0, an application program of (Ghiorso and Evans 2008), using chemical compositions of selected magnetite and ilmenite pairs that passed the (Bacon and Hirschmann 1988) test (Fig. 7a). The estimated temperatures cluster around 780 °C (Fig. 7c) and oxygen fugacity between 0.5 and 1.0 log₁₀ fO₂ Δ NNO (Fig. 7b). The temperature observed is consistent with the previous report by Ui 1971 (770–780 °C) (model: Buddington and Lindsley 1964). The fact that the chemical diffusion rate in Fe–Ti minerals is fast (Nakamura 1995; Venezky and Rutherford 1999) indicates that this temperature (780 °C) is indicative of the temperature of erupted

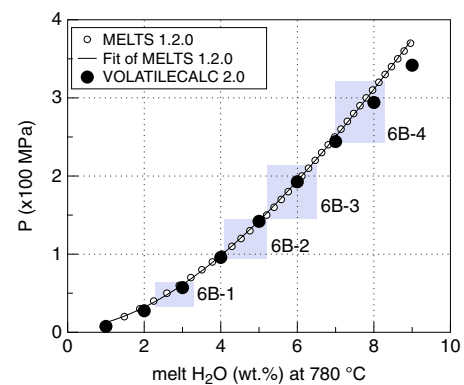


Fig. 8 Water solubility of Hj J-Q melt from MELTS computations. Open circles: water concentration in melt of Hj J-Q at 780 °C extracted from the MELTS output. Thin curve: fitting of the MELTS data ($y = 0.035x + 0.057x^2 - 0.0017x^3 + 0.035$). Solid circles: water concentration in rhyolite melt at 780 °C by VOLATILECALC (Newman and Lowenstern 2002). Shaded areas represent the observed ranges of water concentration in melt of Hijiori (peaks shown in Fig. 6b-1, -2, -3, -4) and the corresponding pressure

magma, rather than those temperatures of magma existed long before the eruption, in either above models.

Pressure (depth)

The pressure (depth) of the Hijiori magmas was estimated using two different ways (Table 2). First, the concentration of H₂O in MIs yields a minimum trapping pressure estimate. Water solubility data of Hj J-Q melt extracted

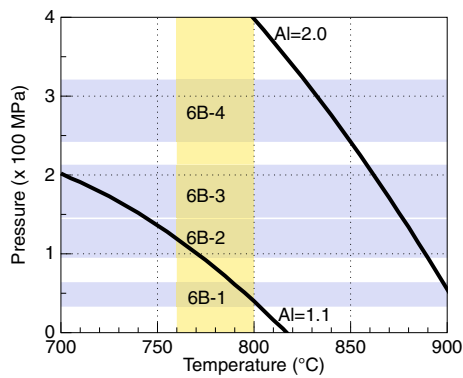


Fig. 9 Aluminum concentration in hornblende. *Thick curves* pressure–temperature dependence of Al in hornblende (normalized to 15 cation atoms per formula unit) by Anderson and Smith (1995). *Gray shaded areas* observed ranges of water concentration in melt of Hijiori (peaks shown in Fig. 6b-1, b-2, b-3, b-4) and the corresponding pressure. *Yellow shaded area* estimated magmatic temperature of Hijiori (Fig. 7c)

Table 2 Pressure (depth) estimation

Method	Data (Figures)	H ₂ O (wt%)	Pressure (MPa)	Depth (km)
H ₂ O in MIs (wt% H ₂ O)	6B-1	2.3–3.3	33–64	1.3–2.6
	6B-2	4.1–5.2	95–145	3.8–5.8
	6B-3	5.2–6.5	145–213	5.8–8.5
	6B-4	7.0–8.3	242–321	9.7–13
Al-in-Hb (Al p.f.u.)	4B-1	1.1	82±60	3.3±2.4
	4B-3	2.0	451±60	18±2.4

from the MELTS output yielded saturation pressures of 33–64, 95–145, 145–213, and 242–321 MPa, for the observed melt H₂O peaks shown in Fig. 6b-1 (2.3–3.3 wt%), 6b-2 (4.1–5.2 wt%), 6b-3 (5.2–6.5 wt%), and 6b-4 (7.0–8.3 wt%), respectively, at the temperature of 780°C (Fig. 8). Assuming a lithostatic gradient of 4 km/100 MPa, the 6b-1, 6b-2, 6b-3, and 6b-4 peaks in Fig. 6b would correspond to depths of 1.3–2.6, 3.8–5.8, 5.8–8.5, and 9.7–13 km, respectively. The variation in pressures can be interpreted as follows. A small number of quartz and hornblende phenocrysts trapped MIs at 242–321 MPa (9.7–13 km). This was followed by higher K₂O (3.8 wt%, Fig. 6a-3) melts trapped in plagioclase phenocrysts at 145–213 MPa (5.8–8.5 km). Quartz and mafic phenocrysts then trapped melts with lower K₂O concentrations (3.5 wt%, K₂O, Fig. 6a-2) at 95–145 MPa (3.8–4.8 km). The last stage of trapping involved the crystallization of mafic minerals that included MIs at shallower levels (33–64 MPa or 1.3–2.6 km) but a series of drill core data indicate the depth should not be shallower than 1.5 km where the basement of the

regional Neogene sedimentary rocks is located. This indicates that the Hijiori magma plumbing system may be vertically elongated (>10 km).

The second method of pressure estimation used in this study involves the relationships between aluminum concentration in hornblende, temperature, and pressure by Anderson and Smith (1995) (Fig. 9). However, the Anderson and Smith barometer should be used with caution since this is a best fit to previous empirical calibrations (Hammarstrom and Zen 1986; Hollister et al. 1987; Johnson and Rutherford 1989; Schmidt 1992) which, besides temperature, required also a buffering assemblage. The aluminum concentrations in hornblende peak at 1.1 Al pfu and range between 1.0 and 2.0 Al pfu (Fig. 4b).

A magma temperature of 780°C yields pressures of 82±60 MPa (3.3±2.4 km) for 1.1 Al pfu and 451±60 MPa (18±2.4 km) for 2.0 Al pfu. The presence of Al-rich cores surrounded by Al-poor rims may suggest that hornblende crystallization took place sequentially at different depths and/or temperatures, for instance, either crystallization begun at a higher temperature and ended at a lower temperature or crystallization took place in depth and ended at a shallower place. Hornblende crystallization at different depths is consistent with the interpretation of the observed wide variation in MI H₂O concentrations discussed above, since the crystallization and melt inclusion also occurred at 242–321 MPa (9.7–13 km) (Table 2). Besides, the presence of patchy calcic plagioclase and aluminous hornblende aggregates (Fig. 2f, g) suggests that dissolution of albite-rich plagioclase and crystallization of hornblende may also have occurred at temperatures higher than those estimated from Fe–Ti oxides (780 °C). In this case the pressure using the aluminous hornblende (Table 2: 451±60) will be overestimated. The majority of hornblende phenocrysts are aluminum poor (Fig. 4), these minerals may crystallize at 82±60 MPa (3.3± km). In addition, the observed H₂O concentration of MIs in hornblende phenocrysts is relatively low (Fig. 6b-1). Therefore, we conclude that the pressure of hornblende crystallization is 82±60 MPa (3.3±2.4 km). Again, a series of drill core data indicate the depth should not be shallower than 1.5 km.

Magma melt fractions

Magma melt fractions were estimated using two different methods. The first method involved determining the mass fractions of melt and phenocrysts (plagioclase (pl), hornblende (hb), quartz (qz), magnetite (mt), ilmenite (il), and orthopyroxene (opx)) shown in Table 1, followed by the calculation of the weighted average [wr(calc)] of these components to reproduce the observed bulk rock composition (wr). This least squares modeling indicates that the magma

consists of melt (43 wt%), plagioclase (38 wt%), hornblende (11 wt%), quartz (3.6 wt%), magnetite (3.4 wt%), ilmenite (0.4 wt%), and orthopyroxene (0.3 wt%) (Table 1).

The second method estimates the magma melt fraction by assessing the degree of accumulation of incompatible elements in the melt. The potassium concentrations in bulk rock and melt obtained in this study, 1.7 and 3.6 wt%, respectively, yield an estimate melt fraction of 48 wt%, assuming that potassium remains in the melt during crystallization. Variations in potassium concentrations (1.5–1.9 wt% K_2O in bulk rock, and 3.3–4.0 in MIs) suggest that the melt fraction may vary between 38 and 59 wt%. This melt fraction may be overestimated since both plagioclase and hornblende

take up some K_2O (~0.3 wt%, Table 1); therefore, potassium concentration in the melt should decrease. The MELTS computation suggests melt fraction of 43–44 wt% to contain melt K_2O concentration as high as 3.5–3.6 wt%. These values are comparable to the mass balance-derived estimates (43 wt%, Table 1). Thus, the crystal fraction of magma (100-melt) of Hijiori is estimated to be 53~57 wt%.

Amount of bulk magmatic H_2O

Since H_2O concentrations in MIs are affected by both vapor saturation and magma crystallization, the observed values do not simply represent bulk magmatic H_2O concentrations (e.g., Papale 2005). Given this, bulk magmatic H_2O concentrations were estimated using the effect of water on the amount and chemical composition of phenocrysts and melt by comparing the observed temperatures, pressures, and crystal content with the results of modeling using MELTS.

The first step of this method is to determine the abundance of quartz crystals;

The amount of quartz in equilibrium with Hijiori magma is shown in Figure 10, where three models involving bulk water contents of 0.5, 2.5, and 5.0 wt% are employed. The stability field of quartz decreases with addition of water (Fig. 10a → b → c), and quartz abundances reach a minimum at pressures of approximately 30, 150, and 400 MPa for bulk water contents of 0.5, 2.5 and 5.0 wt%, respectively. The higher the bulk H_2O content, the lower the minimum quartz abundance. Change in fO_2 from FMQ to FMQ+2 log unit resulted in negligible change on the amount of quartz (Miyagi 2011). The results of MELTS computations are linked with the following observations or determinations: (1) the estimated temperature of Hijiori magma is approximately 780°C (Fig. 7), (2) quartz phenocryst-hosted MIs have H_2O concentrations that are indicative of trapping at pressures of 145–213 MPa (Fig. 6b-3, 5.2–6.5 wt% H_2O), (3) the quartz phenocrysts crystallized during magma ascent (Fig. 2d), and (4) the abundance of quartz in the Hijiori magma is 3.6 wt% (Table 1). These combined factors yield a best-fit bulk H_2O value of around 2.5 wt% H_2O (Fig. 10b). The high quartz abundance in the analyzed samples indicates that 0.5 wt% H_2O is too small for the bulk magmatic water content (Fig. 10a). In addition, 5.0 wt% H_2O is too much as no quartz will crystallize at pressures above about 150 MPa (Fig. 10c). A bulk magmatic H_2O value of 2.5 wt% (Fig. 10b) combined with a quartz abundance of 3.6 wt% and a magmatic temperature of 780°C yields pressures around 150 MPa, which is consistent with the water pressures identified from quartz phenocryst-hosted MI H_2O concentrations. There is a quartz liquidus minimum at approximately 200 MPa, probably explain the observed dissolution and recrystallization textures (Fig. 2d). Similar results are also achieved with a bulk H_2O concentration of 3.0 wt%. Taken

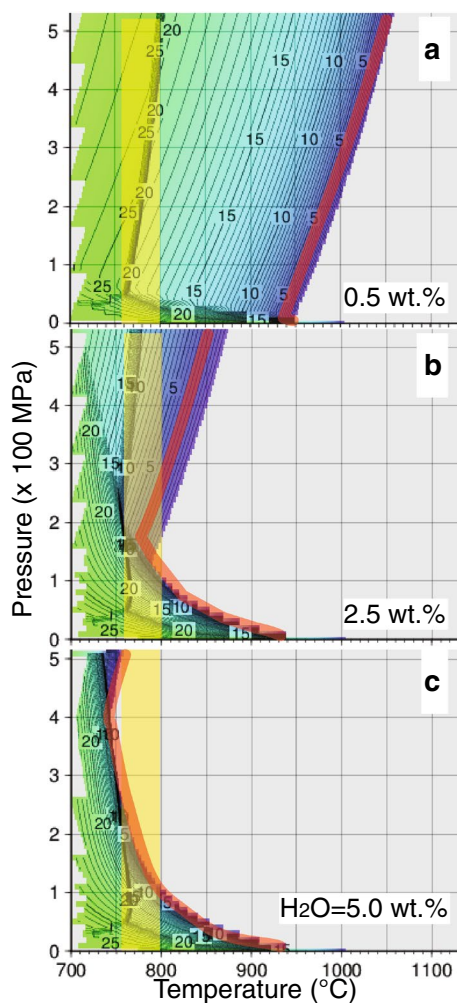


Fig. 10 Abundances of quartz in equilibrium with the Hijiori magma. The abundances of quartz (wt%) were summarized in a series of pressure–temperature plane contour maps showing the cases' bulk magmatic H_2O = 0.5 wt% (a), 2.5 wt% (b), and 5.0 wt% (c). The yellow mark represents the observed magmatic temperature (780 °C, Fig. 7), and the red curve the estimated quartz mode (3.6 wt%, Table 1)

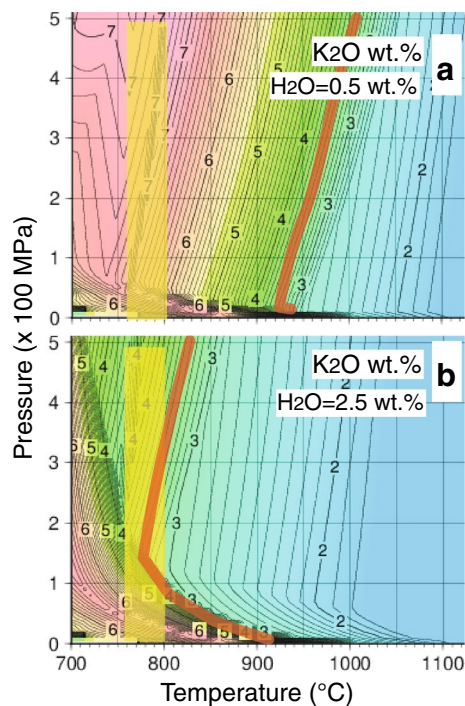


Fig. 11 K_2O concentration of melt in equilibrium with the Hijiori magma. The K_2O concentrations of melt (wt%) was summarized in a series of pressure–temperature plane contour maps showing the cases’ bulk magmatic $H_2O = 0.5$ wt% (a) and 2.5 wt% (b). The yellow mark represents the observed magmatic temperature (780 °C, Fig. 7), and the red curve the observed K_2O concentration in melt (3.55 wt%, Table 1; approximately 3.5 wt%, Figure 6a-2; 3.8 wt%, Figure 6a-3)

together, we guess the bulk H_2O concentration in the Hijiori magma to be between 2.5 and 3.0 wt%.

The second method uses melt K_2O concentrations to estimate the bulk H_2O concentration of Hijiori magma.

Figure 11 shows the K_2O concentration of melt in equilibrium with the Hijiori magma for bulk water contents of 0.5 and 2.5 wt%. The melt K_2O concentrations decrease with addition of water (Fig. 11a → b). A magmatic temperature of 780°C, pressure of 150 MPa, and melt K_2O concentrations ranging from 3.5 wt% (Fig. 6a-2) to 3.8 wt% (Fig. 6a-3) yield a bulk H_2O value of 2.5 wt% (Fig. 11b) where the observed and calculated K_2O concentrations match.

The third method employs anorthite compositions of plagioclase phenocrysts.

Figure 12 shows anorthite compositions (0–1 An mol) of plagioclase in equilibrium with the Hijiori magma for bulk water contents of 2.5 and 5.0 wt%. Plagioclase An compositions positively correlate with water concentrations (Fig. 12a → b). Exploiting this feature, with a magmatic temperature of 780°C, pressure of >50 MPa, and an

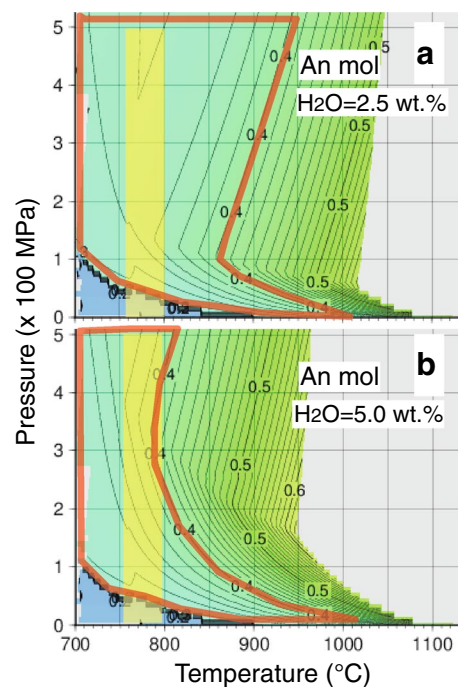


Fig. 12 Anorthite composition of feldspar in equilibrium with the Hijiori magma. Anorthite compositions (An#; 0–1 mol fraction) of feldspar was summarized in a series of pressure–temperature plane contour maps showing the cases’ bulk magmatic $H_2O = 2.5$ wt% (a) and 5.0 wt% (b). The yellow region represents the observed magmatic temperature (780 °C, Fig. 7), and the region surrounded by red border is the observed K_2O concentration in melt (30–40 mol%, Figure 4a)

anorthite composition of 0.3–0.4 (Fig. 4a-1), the bulk H_2O value approaches 2.5 wt% (Fig. 12a), where observed and calculated anorthite values quantify match.

The plagioclase compositions may also record a hidden high-temperature magmatic component. For instance, An compositional peaks are present at 0.52–0.58 (Fig. 4a-2) and 0.6–0.7 (Fig. 4a-3). These higher An values were found in the core, patchy reaction bands, and rims of plagioclase phenocrysts (Fig. 2a-L, b-L). The peak shown in Fig. 4a-2 has a closely similar anorthite composition to the near-plagioclase liquidus (An 0.52–0.58: Fig. 12a, 1000 °C, 50–300 MPa). These P–T– H_2O conditions suggest the input of a new batch of magma into the shallow magma chamber of Hijiori.

Similarly, peak 2 and peak 3 in Fig. 4a are comparable to the near-liquidus peaks (An \approx 0.62: Fig. 12b, bulk $H_2O=5.0$ wt%, 900°C–950 °C and 100–200 MPa). These conditions may indicate mixing of the new magma and the existing magmatic mush yielding intermediate temperatures and low concentrations of H_2O . The observed maximum An composition (\approx 0.7, Fig. 4a-4) was not reproduced by the MELTS modeling of the bulk Hijiori magma

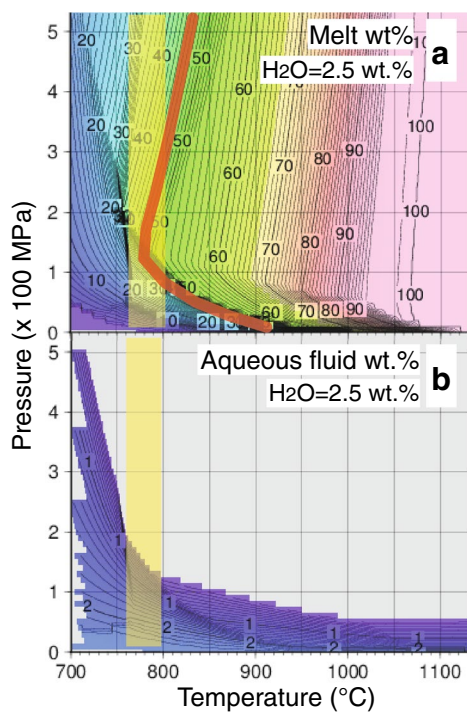


Fig. 13 Amount of melt (a) and fluid (b) in equilibrium with the Hijiori magma. The amount of melt (wt%) and fluid (wt%) were summarized in a suite of pressure–temperature plane contour maps showing the cases’ bulk magmatic $\text{H}_2\text{O} = 2.5$ wt%. The yellow mark the observed magmatic temperature (780 °C, Fig. 7), and the red curve the observed melt fraction (43.27 wt%, Table 1; 43–44 wt%, see discussion in “Magma melt fractions”)

compositions, suggesting that a more mafic magma may have been present in the system. This also suggests that the magma mixing at Hijiori included not only (1) chemically identical hot aphyric dacite but also (2) a trace amount of a more mafic end-member that did not cause significant compositional variation in the whole rock chemistry of Hijiori eruptive products. It is noteworthy that the melt fraction of the magma will be approximately 70 wt% at temperature of 900 °C, water content at 2.5 wt% H_2O and pressure at 100–200 MPa (Fig. 13a). Less viscous magma with that temperature would be able to move upward through the immobile mush body towards shallow storage areas before the magma finally cooled to the observed pre-eruptive magmatic temperature of approximately 780 °C.

As mentioned above, magma temperatures greater than 780 °C mean that the Al-rich hornblende-based pressure values determined in this study (≈ 320 MPa) could be over-estimated. In fact, some of the Al-rich hornblende crystallized simultaneously with plagioclase dissolution and re-crystallized (Fig. 2f) at pressures of 145–243 MPa, as estimated from plagioclase-hosted MI H_2O concentrations

(Table 2, Fig. 6b-3). Pressures between 145 and 243 MPa yield hornblende crystallization temperatures of 860–880 °C (Fig. 9). We guess that hornblende phenocrysts with Al-rich cores may have crystallized from a new magma after cooling to 860–880 °C, whereas hornblende phenocrysts with Al-poor cores may have formed in the hybrid magma after being rapidly transported to a shallow but large storage area a few kilometers deep where the temperature was probably constant (approximately 780 °C).

Conditions of magma storage for a new volcano

The bulk rock major chemistry, water contents, and temperatures outlined above mean that MELTS modeling can be used to determine the physical parameters of the system.

The chemical mass balance calculations and MELTS modeling undertaken during this study indicated that the erupted upper portion of the Hijiori magmatic plumbing system was located at depths of 2–4 km and had the following characteristics: (1) bulk magmatic H_2O was approximately 2.5 wt%, (2) crystal content was ≤ 57 vol%, (3) bulk modulus was about 0.1–0.8 GPa, (4) density was between 1.8 and 2.3 g/cc, and (5) excess magmatic H_2O was 11–32 vol% or 48–81 mol% (Table 3). Drill core data by NEDO indicated that the Hijiori caldera had undergone piston-cylinder-type subsidence (Miyagi 2007; NEDO 1983), suggesting that the depth of the deflation source, i.e., the depth of magma chamber, beneath the Hijiori caldera is thought to be relatively shallow. Upper limit of the depth will be ≈ 1.5 km, above which Neogene sedimentary rocks are recovered by the drill core. The top of the magma chamber may be comparable to or smaller than the diameter of the caldera, about 2 km, located approximately at a depth of 2–4 km or greater, which probably corresponds to the shallowest depth of the final hornblende crystallization, and to low-density (< 2.3 g/cc), highly solidified (> 57 wt%), and highly vesicular (> 32 vol% H_2O) magmas (Table 3, Fig. 14). Both bulk modulus (K) and density (ρ) of magma are important parameters to estimate pressure wave velocity ($V_p = \sqrt{K/\rho}$) in the magma. Bulk modulus of the Hijiori dacite with 2.5 wt% H_2O changes abruptly across a depth of 6 km in response to water saturation (Table 3). The more the amount of magmatic water, the greater the water saturation depth.

As discussed above, the crystal fraction of magma (100-melt) of Hijiori is estimated to be 53–57 wt%. Magmas with crystallinity more than ~ 50 vol% are considered to be nearly uneruptible (Gottsmann et al. 2009; Marsh 1981; Scaillet et al. 1998). The range of estimated pressure (depth) of the Hijiori magma is relatively wide and as shallow as about 50 MPa (~ 2 km) (Fig. 8). Because of excess water fluid

Table 3 Physical parameters obtained from MELTS computations

P	Depth	Rho	K	Solid		Fluid	
				wt%	vol%	vol%	mol%
10	0.4	0.7	0.0	96	23	76	99
20	0.8	1.1	0.0	93	37	61	97
30	1.2	1.4	0.1	89	46	49	93
40	1.6	1.6	0.1	82	49	39	85
50	2.0	1.8	0.1	79	53	32	81
60	2.4	1.9	0.2	76	55	26	75
70	2.8	2.1	0.3	73	57	22	69
80	3.2	2.1	0.4	70	57	18	63
90	3.6	2.2	0.6	67	57	14	56
100	4.0	2.3	0.8	64	56	11	48
110	4.4	2.3	1.2	60	55	9	39
120	4.8	2.4	1.8	57	53	6	30
130	5.2	2.4	3.1	53	51	4	19
140	5.6	2.4	6.5	49	50	2	8
150	6.0	2.5	16	46	48	0	0
160	6.4	2.5	16	47	47	↓	↓
170	6.8	2.5	16	47	47		
180	7.2	2.5	17	47	47		
190	7.6	2.5	17	48	48		
200	8.0	2.5	17	48	48		
210	8.4	2.5	17	49	48		
220	8.8	2.5	17	49	49		
230	9.2	2.5	17	49	49		
240	9.6	2.5	17	50	50		

Temperature, oxygen fugacity, and bulk H₂O content of the system was set to be 780 °C, FMQ+2 log unit, and 2.5 wt%, respectively. The figures of depth give tentative criteria, which are simply calculated assuming a lithostatic gradient of 4km/100MPa

(bubbles) in such a shallow magma, the crystal volume fraction will be lowered, while the melt dehydration will increase with a solid weight fraction. As a result, there is a local maximum of crystal volume fraction at some depth, e.g., around 3 km for the Hijiori magma with bulk H₂O = 2.5 wt% (Table 3). The crystal volume fraction of the Hijiori magma is less than 50 vol.% at either depth <1.6 km (40 MPa) or >5.6 km (140 MPa) (Table 3). The pressure dependence of the crystal volume fraction in Hijiori suggests that the magma is still eruptible at a depth of <1.6 or >5.6 km where the crystal volume fraction will be less than 50 vol%. A magma with 48 ±3 vol% phenocrysts actually erupted at the Hokkaido-Komagatake volcano in 1929 (Takeuchi and Nakamura 2001). In addition, a rapid magma decompression probably initiated magma fragmentation (Dingwell 1996; Spieler et al. 2004; Alidibirov and Dingwell 2000) of the uneruptible part of the Hijiori magma. That magma fragmentation is probably the reason why the

larger plagioclase phenocrysts of Hijiori generally occurs as broken fragments.

Given that the magma plumbing system of Hijiori consists of an immobile mush, we suggest that magma transportation occurred primarily as an injection of hot and less viscous magma into the mush. This injection can occasionally re-mobilize the mush. The melt fraction of the re-mobilized or hybrid magma can be as high as 70 wt% at 900 °C (Fig. 13a). The textures and chemical compositions of the An-rich plagioclase and Al-rich hornblende aggregates (Fig. 2-f, -g) suggest that the plagioclase phenocrysts crystallized after partial dissolution at the depth of 5.8–8.5 km (Table 2, Fig. 6b-3) and at the temperature of 900–1000 °C during mingling with the pre-existing mushy magma. The crystallization of Al-rich hornblende may be contemporaneous with that of An-rich plagioclase at slightly lower temperatures (860–880 °C; see 6B-3 and Al=2.0 in Fig. 9). On the other hand, the majority of Al-poor hornblende may be

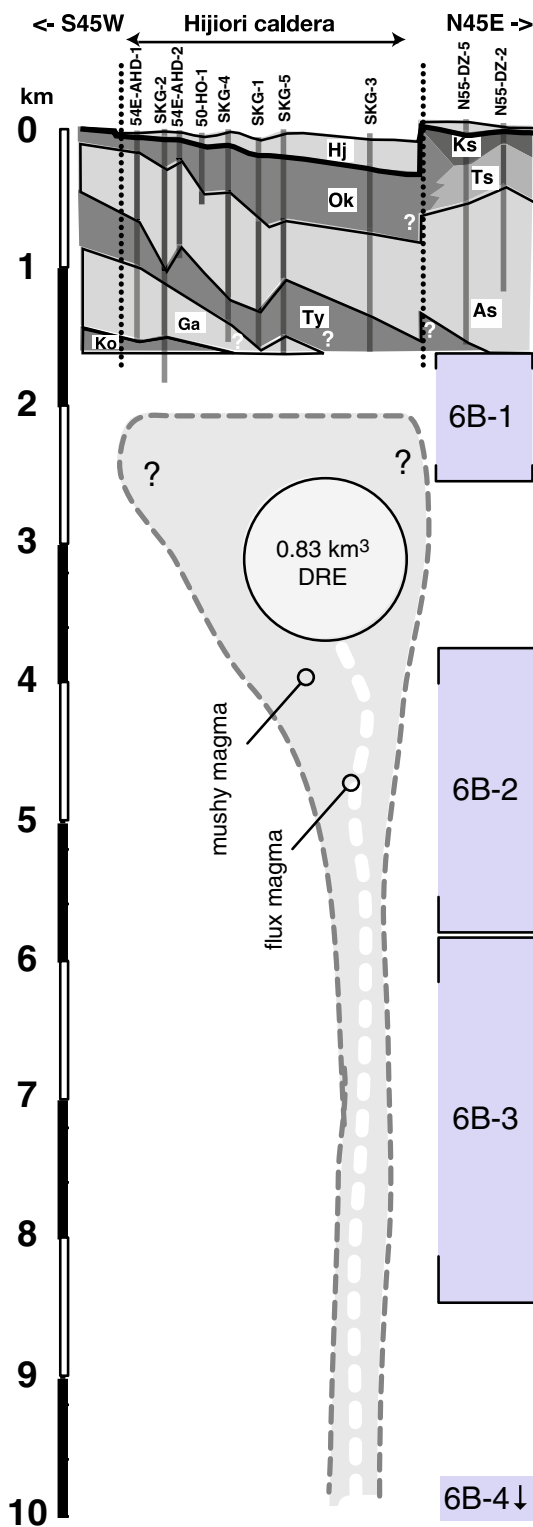


Fig. 14 Magma plumbing system of Hijiori volcano. A geological section is shown in an aspect ratio of 1:1. Identifiers of the location of drillings by (NEDO 1983) are shown above the surface of the geological section. The section through 0–1.6 km below surface is modified after Miyagi (2007), based on the drilling data of NEDO (1983). *Ko* Kodake granite, *Ga* Gassan Formation (F.) (altered basalt and andesite), *Ty* Tatsuyazawa F. (mudstone and tuff), *As* Aosawa F. (basalt), *Ok* Okkura acidic tuff F., *Ts* Tsunokawa F. (mudstone), *Ks* Kusanagi F. (shale), *Hj* Caldera fill of Hijiori. A sphere entitled “0.83 km³ DRE” shows the erupted volume of Hijiori (Miyagi 2007). Estimated depths of the magma plumbing system are shown as 6B-1, -2, -3, -4 (see Table. 2; Figs. 8 and Fig. 10)

plumbing system at depth and a relatively wide shallower magma storage system with a volume greater than the total erupted volume of Hijiori (at least 0.83 km³, shown as a section of sphere in Fig. 14).

Summary

This study documents the bulk rock chemistry of pumices, the chemical compositions of phenocrysts and melt inclusions and discusses the temperatures, pressures, crystal content, and amounts of bulk magmatic H₂O in the Hijiori magmatic system; the study also applies MELTS modeling to determine the physical parameters of the magmatic plumbing system. The bulk rock compositions are dacitic with SiO₂ concentrations mostly of 66 ± 1.5 wt%. The major element chemistries and textures of plagioclase and hornblende phenocrysts suggest that repeated magma mixing occurred before eruption. The observed chemical compositions of Fe–Ti minerals suggest the temperature of magma to be approximately 780°C. Melt inclusion H₂O concentrations suggest that the majority of inclusions were trapped at depths between 3.8 and 8.5 km with a small number of inclusions in quartz and hornblende phenocrysts at depths of 9.7–13 km and some inclusions in orthopyroxenes at shallower depths of 1.5–2.6 km. The aluminum content in hornblende along with the H₂O content in melt inclusions in hornblende phenocrysts suggest that the mineral began to crystallize at depths of 9.7–13 km although the majority of hornblende was formed at depths of 3.3 ± 2.4 km. The results of chemical mass balance calculations and MELTS modeling indicate that the erupted uppermost part of the Hijiori magma plumbing system had (1) a magma crystal content of ≤57 vol%, (2) contained a bulk magmatic H₂O concentration of approximately 2.5 wt%, and (3) contained excess magmatic H₂O of 11–32 vol% or 48–81 mol%. These data also indicate that repeated input of felsic magma led to the formation of a >0.83 km³ vapor-rich and crystal-rich magma chamber at a depth of approximately 2–4 km. The above physical parameters are required for the geophysical investigation techniques to detect magma chambers prior to the first, small caldera-forming eruption of Hijiori volcano.

formed in a shallow storage with a temperature of approximately 780°C and a depth of 3.3 ± 2.4 km or 82 ± 60 MPa (see 6B-1 and AI=1.1 in Fig. 9) after relatively rapid transportation. This rapid transportation favors a relatively narrow magma path. Thus, we propose a relatively slim magma

Acknowledgements We thank Dr. T. Yamamoto for providing the opportunity to undertake this study, Dr. T. Matsu'ura for fruitful discussions during fieldwork, Dr. T. Ohtani for the help on cathode-ray luminescence observation using his luminoscope, Dr. N. Hoang and Mr. N. Steinau for helpful comments on manuscript, and Dr. T. Hokada for his help on cathode-ray luminescence imaging; constructive comments and encouragements from Dr. C. Miller, Dr. G. Gualda, Dr. B. Scaillet, Dr. G. Zellmer, Dr. M. J. Rutherford, and anonymous reviewers improved the quality of the manuscript; Ms. R. Oikawa, T. Yamaguchi, and K. Asaoka for assistance during sample preparation. This research project was conducted as the regulatory supporting research funded by the Secretariat of Nuclear Regulation Authority (Secretariat of NRA), Japan.

Open Access This article is distributed under the terms of the Creative Commons Attribution 4.0 International License (<http://creativecommons.org/licenses/by/4.0/>), which permits unrestricted use, distribution, and reproduction in any medium, provided you give appropriate credit to the original author(s) and the source, provide a link to the Creative Commons license, and indicate if changes were made.

References

- Alidibirov M, Dingwell D (2000) Three fragmentation mechanisms for highly viscous magma under rapid decompression. *J Volcanol Geotherm Res* 100:413–421
- Anderson JL, Smith DR (1995) The effects of temperature and fO_2 on the Al-in-hornblende barometer. *Am Mineral* 80:549–559
- Asimow P, Ghiorso M (1998) Algorithmic modifications extending melts to calculate subsolidus phase relations. *Am Mineral* 83:1127–1131
- Bacon CR, Hirschmann MM (1988) Mg/mn partitioning as a test for equilibrium between coexisting Fe-Ti oxides. *Am Mineral* 73(1–2):57–61
- Begue F, Ghiorso GAR, Ghiorso MS, Pamukcu AS, Kennedy BM, Gravey DM (2014) Phase-equilibrium geobarometers for silicic rocks based on rhyolite-MELTS. Part 2: application to Taupo volcanic zone rhyolites. *Contrib Mineral Petrol* 168(1082):1–16. doi:10.1007/s00410-014-1082-7
- Borisova AY, Pichavant M, Beny JM, Pronost J (2005) Constraints on dacite magma degassing and regime of the June 15, 1991, climatic eruption of Mount Pinatubo (Philippines): new data on melt and crystal inclusions in quartz. *J Volcanol Geotherm Res* 145:35–67
- Buddington A, Lindsley D (1964) Iron-titanium oxide minerals and synthetic equivalents. *J Pet* 5:310–357
- Devine JD, Gardner JE, Brack HP, Layne GD, Rutherford MJ (1995) Comparison of microanalytical methods for estimating H_2O contents of silicic volcanic glasses. *Am Mineral* 80:319–328
- Dingwell DB (1996) Volcanic dilemma: flow or blow? *Science* 273:1054–1055
- Ghiorso MS, Evans BW (2008) Thermodynamics of rhombohedral oxide solid solutions and a revision of the Fe-Ti two-oxide geothermometer and oxygen-barometer. *Am J Sci* 308(9):957–1039
- Ghiorso MS, Sack RO (1995) Chemical mass transfer in magmatic processes IV. A revised and internally consistent thermodynamic model for the interpolation and extrapolation of liquid-solid equilibria in magmatic systems at elevated temperatures and pressures. *Contrib Mineral Petrol* 119:197–212
- Gottsmann J, Lavallée Y, Martí J, Aguirre-Díaz G (2009) Magma-tectonic interaction and the eruption of silicic batholiths. *Earth Planet Sci Lett* 284(3–4):426–434
- Gualda GAR, Ghiorso MS (2013) Low-pressure origin of high-silica rhyolites and granites. *J Geol* 121(5):537–545
- Gualda GAR, Ghiorso MS, Lemons RV, Carley TL (2012) Rhyolite-MELTS: a modified calibration of MELTS optimized for silica-rich, fluid-bearing magmatic systems. *J Petrol* 53(5):875–890
- Hamada M, Fujii T (2007) H_2O -rich island arc low-K tholeiite magma inferred from Ca-rich plagioclase-melt inclusion equilibria. *Geochem J* 41:437–461
- Hammarstrom JM, Ea Zen (1986) Aluminium in hornblende: an empirical igneous geobarometer. *Am Mineral* 71:1297–1313
- Hasegawa K, Suzuki M (1964) 1:50,000 Geological map of Hokkaido, Goryokaku with explanatory Text. *Geol Survey Hokkaido* 86 (in Japanese with English abstract)
- Hauri E, Wang J, Dixon JE, King PL, Mandeville CW, Newman S (2002) SIMS analysis of volatiles in silicate glasses 1. Calibration, matrix effects and comparisons with FTIR. *Chem Geol* 183:99–114
- Hollister LS, Grissom GC, Peters EK, Stowell HH, Sisson V (1987) Confirmation of the empirical correlation of al in hornblende with pressure of solidification of calc-alkaline plutons. *Am Mineral* 72:231–239
- JMA (2013) National catalogue of the active volcanoes in Japan, vol 4. Japan Meteorological Business Support Center, Tokyo (in Japanese)
- Johnson MC, Rutherford MJ (1989) Experimental calibration of the aluminium-in-hornblende geobarometer with application to long valley caldera (california) volcanic rocks. *Geology* 17:837–841
- Kanisawa S, Yoshida T (1989) Genesis of the extremely low-K tonalites from the island arc volcanism. Lithic fragments in the Adachi-Medeshima pumice deposits Northeast Japan. *Bull Volcanol* 51:346–354
- Kano K, Ohguchi T, Yanagisawa Y, Awata Y, Kobayashi N, Sato Y, Hayashi S, Kitazato H, Ogasawara K, Komazawa M (2011) Geology of the Toga and Funakawa district. *Quadrangle Series* 1:50,000, 2nd edn, vol 6 Akita. Geological Survey of Japan, AIST, Japan, p 127
- Katsui Y, Yamamoto M, Nemoto S, Niida K (1979) Genesis of calc-alkaline andesite from Oshima-oshima and Ichinomegata volcanoes, north Japan. *J Fac Sci Hokkaido Univ Ser IV* 19:157–168
- Kawaguchi Y, Murakami H (1994) Types and formation processes of pyroclastic flow deposits distributed in the Hiziori area, Yamagata Prefecture. *Rept Res Inst Nat Resour Min Coll Akita Univ* 15:81–88 (in Japanese with English abstract)
- Marsh BD (1981) On the crystallinity, probability of occurrence, and rheology of lava and magma. *Contrib Mineral Petrol* 78(1):85–98
- Miyagi I (2004) On the eruption age of the Hijiori caldera, based on more accurate and reliable radiocarbon data. *Bull Volcanol Soc Japan* 49(4):201–205
- Miyagi I (2007) Stratigraphy and volcanic activities of Hijiori volcano, Northeastern Japan arc. *Bull Volcanol Soc Japan* 52(6):311–333 (in Japanese with English abstract)
- Miyagi I (2011) Contour maps of some useful petrological parameters on P-T plane: a case of Hijiori volcano, NE Japan. *Open File Report of GSJ*, p. 534 <https://www.gsj.jp/data/openfile/no0534/index.html>
- Miyagi I, Yurimoto H (1995) Water content of melt inclusions in phenocrysts using secondary ion mass spectrometer. *Bull Volcanol Soc Japan* 40:349–355
- Miyagi I, Itoh J, Hoang N, Morishita Y (2012) Magma systems of the Kutcharo and Mashu volcanoes (NE Hokkaido, Japan): petrogenesis of the medium-K trend and the excess volatile problem. *J Volcanol Geotherm Res* 231–232:50–60
- Miyashiro A (1974) Volcanic rock series in island arcs and active continental margins. *Am J Sci* 274:321–355
- Murakami H, Kawaguchi Y (1994) Chemical variability in hornblendes related to volcanic activity of Hiziori caldera, Yamagata Prefecture. *Rept Res Inst Nat Resour Min Coll Akita Univ* 59:1–23 (in Japanese with English abstract)

- Nakamura M (1995) Continuous mixing of crystal mush and replenished magma in the ongoing unzen eruption. *Geology* 23:807–810
- Nakamura M, Shimakita S (1998) Dissolution origin and syn-entrapment compositional change of melt inclusion in plagioclase. *Earth Planet Sci Lett* 161:119–133
- NEDO (1983) The lower Dozan river. Technical report No. 2. New Energy and Industrial Technology Development Organization (**in Japanese**)
- Newman S, Lowenstern JB (2002) VolatileCalc: a silicate melt-H₂O-CO₂ solution model written in visual basic for excel. *Comput Geosci* 28:597–604
- NIED (2013) Technical note of the national research institute for earth science and disaster prevention. Volcanic hazard maps of Japan, 2nd edn, vol 380. National Research Institute for Earth Science and Disaster Prevention, Japan, p 186
- Papale P (2005) Determination of total H₂O and CO₂ budgets in evolving magmas from melt inclusion data. *J Geophys Res* 110(B03208):1–13. doi:10.1029/2004JB003033
- Scailliet B, Holtz F, Pichavant M (1998) Phase equilibrium constraints on the viscosity of silicic magmas: 1. Volcanic-plutonic comparison. *J Geophys Res Solid Earth* 103(B1110):27257–27266
- Schmidt MW (1992) Amphibole composition in tonalite as a function of pressure: an experimental calibration of the Al-in Hornblende barometer. *Contrib Mineral Petrol* 110:304–310
- Skirius CM, Peterson JW, Anderson J, Alfred T (1990) Homogenizing rhyolitic glass inclusions from the bishop tuff. *Am Mineral* 75:1381–1398
- Spieler O, Kennedy B, Kueppers U, Dingwell DB, Scheu B, Taddeucci J (2004) The fragmentation threshold of pyroclastic rocks. *Earth Planet Sci Lett* 226:139–148
- Sugimura A (1953) A Quaternary terrace of pumice flow in the neighbourhood of the volcano Gassan in Japan. *J Geol Soc Jpn* 59:89–91 (**in Japanese with English abstract**)
- Takeuchi S, Nakamura M (2001) Role of precursory less-viscous mixed magma in the eruption of phenocryst-rich magma: evidence from the Hokkaido-Komagatake 1929 eruption. *Bull Volcanol* 63:365–376
- Tamura Y, Tatsumi Y, Zhao D, Kido Y, Shukuno H (2002) Hot fingers in the mantle wedge: new insights into magma genesis in subduction zones. *Earth Planet Sci Lett* 197:105–116
- Tomiya A, Takahashi E (2005) Evolution of the Magma Chamber beneath Usu Volcano since 1663: a Natural Laboratory for Observing Changing Phenocryst Compositions and Textures. *J Petrol* 46(12):2395–2426
- Ui T (1971) Genesis of magma and structure of magma chamber of several pyroclastic flows in Japan. *J Fac Sci Univ Tokyo Sec II* 18:53–127
- Ui T, Sugimura A, Shibahashi K (1973) ¹⁴C age of the Hijiori pyroclastic flow deposit, Northeastern Honshu, Japan. *Bull Volcanol Soc Japan* 18(3):171–172 (**in Japanese with English figure caption**)
- Umeda K, Asamori K, Negi T, Ogawa Y (2006) Magnetotelluric imaging of crustal magma storage beneath the Mesozoic crystalline mountains in a nonvolcanic region, northeast Japan. *Geochem Geophys Geosyst* 7(8):1–8
- Venezky DY, Rutherford MJ (1999) Petrology and Fe–Ti oxide reequilibration of the 1991 Mount Unzen mixed magma. *J Volcanol Geotherm Res* 89:213–230
- Wessel P, Smith W (1998) New, improved version of generic mapping tools released. *EOS Trans Am Geophys U* 79(47):579
- Yamagata K, Machida H, Arai F (1989) Zenikame-Menagawa Tephra: late Pleistocene tephra layers erupted from a submerged vent off the coast of Hakodate, Tsugaru Straits. *Geogr Rev Jpn* 62(A–3):195–207 (**in Japanese with English abstract**)